Original Article

Ex vivo magnetic resonance elastography of the small bowel in Crohn's disease

Florian N. Loch[1]^, Carsten Kamphues[2], Katharina Beyer[1], Christian Schineis[1], Patrick Asbach[3], Rolf Reiter[3,4], Ingolf Sack[3], Jürgen Braun[5]

[1]Charité – Universitätsmedizin Berlin, corporate member of Freie Universität Berlin and Humboldt-Universität zu Berlin, Department of Surgery, Berlin, Germany; [2]Park-Klinik Weißensee, Department of Surgery, Berlin, Germany; [3]Charité – Universitätsmedizin Berlin, corporate member of Freie Universität Berlin and Humboldt-Universität zu Berlin, Department of Radiology, Berlin, Germany; [4]Berlin Institute of Health at Charité – Universitätsmedizin Berlin, BIH Biomedical Innovation Academy, BIH Charité Digital Clinician Scientist Program, Berlin, Germany; [5]Charité – Universitätsmedizin Berlin, corporate member of Freie Universität Berlin and Humboldt-Universität zu Berlin, Institute for Medical Informatics, Berlin, Germany

Contributions: (I) Conception and design: C Kamphues, J Braun, FN Loch, I Sack; (II) Administrative support: J Braun, C Kamphues, K Beyer, P Asbach, C Schineis; (III) Provision of study materials or patients: C Kamphues, J Braun, K Beyer, C Schineis, FN Loch; (IV) Collection and assembly of data: C Kamphues, J Braun, FN Loch, I Sack; (V) Data analysis and interpretation: C Kamphues, J Braun, I Sack, R Reiter, FN Loch; (VI) Manuscript writing: All authors; (VII) Final approval of manuscript: All authors.

Correspondence to: Dr. Florian N. Loch. Charité. Universitätsmedizin Berlin, corporate member of Freie Universität Berlin and Humboldt-Universität zu Berlin, Department of Surgery, Hindenburgdamm 30, 12203 Berlin, Germany. Email: florian.loch@charite.de.

Background: Conventional magnetic resonance enterography is limited in differentiating active inflammation and fibrosis in lesions of Crohn's disease (CD), thus providing a restricted basis for therapeutic decision making. Magnetic resonance elastography (MRE) is an emerging imaging tool that differentiates soft tissues on the basis of their viscoelastic properties. The aim of this study was to demonstrate the feasibility of MRE in assessing the viscoelastic properties of small bowel samples and quantifying differences in viscoelastic properties between healthy ileum and ileum affected by CD.

Methods: Twelve patients (median age: 48 years) were prospectively enrolled in this study between September 2019 and January 2021. Patients of the study group (n=7) underwent surgery for terminal ileal CD, while patients of the control group (n=5) underwent segmental resection of healthy ileum. MRE of ileal tissue samples of surgical specimens from both groups was performed in a compact tabletop MRI scanner. Penetration rate (a in m/s) and shear wave speed (c in m/s) were determined as markers of viscosity and stiffness for vibration frequencies f of 1,000, 1,500, 2,000, 2,500, and 3,000 Hz. Additionally, damping ratio γ was deduced, and frequency-independent viscoelastic parameters were calculated using the viscoelastic spring-pot model.

Results: Penetration rate a was significantly lower in CD-affected ileum compared to healthy ileum for all vibration frequencies ($P<0.05$). Consistently, damping ratio γ was higher in CD-affected ileum, averaged over all frequencies (healthy: 0.58±0.12, CD: 1.04±0.55, $P=0.03$), as well as at 1,000 and 1,500 Hz individually ($P<0.05$). Spring-pot-derived viscosity parameter η was also significantly reduced in CD-affected tissue (2.62±1.37 versus 10.60±12.60 Pa·s, $P=0.02$). No significant difference was found for shear wave speed c between healthy and diseased tissue at any frequency ($P>0.05$).

^ ORCID: 0000-0003-1513-8339.

Conclusions: MRE of surgical small bowel specimens is feasible, allowing determination of viscoelastic properties and reliable quantification of differences in viscoelastic properties between healthy and CD-affected ileum. Thus, the results presented here are an important prerequisite for future studies investigating comprehensive MRE mapping and exact histopathological correlation including characterization and quantification of inflammation and fibrosis in CD.

Keywords: Crohn's disease (CD); magnetic resonance elastography (MRE); fibrosis; active inflammation; magnetic resonance enterography

Submitted Oct 12, 2022. Accepted for publication Feb 23, 2023. Published online Apr 03, 2023.
doi: 10.21037/qims-22-1071
View this article at: https://dx.doi.org/10.21037/qims-22-1071

Introduction

Crohn's disease (CD) and ulcerative colitis (UC) represent the two forms of inflammatory bowel disease (IBD) that are both characterized by inflammation of the gastrointestinal tract (1). Over the last decades, the prevalence of IBD has substantially increased in many countries and regions, which poses a substantial and growing social and economic burden on governments and health systems (2). In patients with CD, symptomatic intestinal strictures are caused by current active inflammation, chronic fibrosis after repeated or persisting inflammation, or a mixture of both active inflammation and fibrosis (3).

The most established and accurate imaging modality for detection of intestinal strictures in CD and treatment planning is magnetic resonance enterography (4). Primarily inflammatory strictures are treated by anti-inflammatory medication, whereas primarily fibrotic strictures require endoscopic intervention or surgery. However, the ability of conventional magnetic resonance enterography to differentiate active inflammation and fibrosis within strictures is limited and, thus, the basis for treatment decisions is restricted (4). Therefore, to ensure sound therapeutic decision making, new imaging techniques that allow exact characterization of CD-affected intestinal tissue are required. A potential candidate is elastography—an image-based tool for the differentiation of soft tissues on the basis of their specific viscoelastic properties (5).

Elastography comprises a medical imaging technique such as magnetic resonance imaging (MRI) or ultrasound (US), mechanical vibrations in the audible range to induce shear waves in the tissue of interest, and inversion algorithms to generate stiffness maps from shear wave patterns (5). In the field of ultrasound elastography (USE), strain elastography (6-10) and shear wave elastography (7,11-14) have been used to determine tissue stiffness. Data from pilot studies suggest that USE can supplement the evaluation of bowel strictures in CD patients for the detection of fibrosis (6-9,11,14) and, in conjunction with other US imaging modalities, contribute to the differentiation of fibrosis and inflammation (9,13).

For magnetic resonance elastography (MRE), a number of studies investigating disorders of abdominal organs such as liver (15-22), spleen (23-25), kidney (26-29), and pancreas (30-34) have been performed. However, studies investigating MRE of the gastrointestinal tract are limited. Initial work has shown that viscoelastic parameters are altered in the inflammatory phase of acute appendicitis (35). Subsequent studies demonstrated the feasibility of *in vivo* intestinal MRE in IBD, reporting altered stiffness in suspected fibrotic CD lesions (36,37). Compared with USE, MRE has higher accuracy due to acquisition of full 3D wave fields (5) and allows straightforward determination of viscosity as an additional potential biomarker for inflammatory diseases (38-40).

In this study, we performed MRE on surgical specimens of healthy terminal ileum and terminal ileum affected by CD using a compact tabletop MRI device that provides volume-based stiffness and viscosity parameters in small tissue samples (41,42). Overall, our study aims at providing reference values for viscoelastic properties of the normal human terminal ileum and investigating how they change in the presence of CD lesions towards the development of MRE as a new imaging modality for exact differentiation of CD lesions.

Methods

Patients

In this prospective single-center study, a total of 12 patients were included. The patients in the study group (n=7)

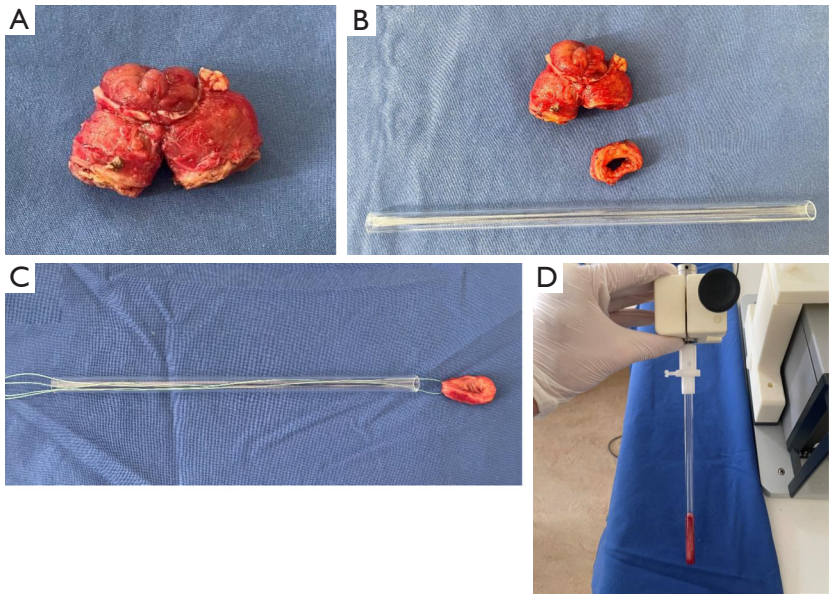

Figure 1 Sample preparation for MRE examination from surgical specimen. (A) Example of entire surgical specimen of a segmental resection of healthy ileum during closure of a protective ileostomy. (B) Removal of a circular segment of ileum from the entire specimen, an empty sample tube is shown in the foreground. (C) Placement of the circular segment of ileum by pulling it into the sample tube using a surgical thread. (D) Sample tube with inserted tissue sample connected to piezo actuator. MRE, magnetic resonance elastography.

underwent surgery due to terminal ileal CD. The patients in the control group (n=5) underwent segmental resection of healthy ileum during closure of a protective ileostomy. All patients underwent surgery at the Department of Surgery, Campus Benjamin Franklin, Charité – Universitätsmedizin Berlin, Germany, between September 2019 and January 2021. Inclusion criteria were an adequate segment of ileum affected by CD in the study group and of healthy ileum in the control group based on macroscopic intraoperative inspection by the study surgeon. Exclusion criterion was an age of <18 years at the time of surgery. The MRE findings in a specimen from a thirteenth patient were excluded due to a defective cable connection between the scanner and the computer. The study was conducted in accordance with the Declaration of Helsinki (as revised in 2013). The study was approved by the ethics committee of the Charité – Universitätsmedizin Berlin (No. EA4/007/19), and written informed consent was obtained from each patient.

Surgical specimens and sample preparation

Patients in the study group underwent either ileocecal resection due to ileocecal CD or resection of an ileotransversostomy in cases with a history of prior ileocecal resection. The control group consisted of patients with segmental resection of healthy ileum during closure of a protective ileostomy. For each patient, the entire surgical specimen was macroscopically inspected directly after removal by the study surgeon to visually identify areas of ileum affected by CD (study group) and healthy ileum (control group). From the areas identified in this way, circular segments of ileum measuring 7.5 mm in width were surgically removed by the study surgeon and prepared for MRE investigation (*Figure 1A*,*1B*). The remaining specimen was formalin-embedded for routine histopathological evaluation. The circular tissue sample was picked up with a surgical thread and carefully transferred into the sample tube (length, 200 mm, outer diameter, 9 mm, inner diameter, 7 mm) (*Figure 1C*). After sealing with plastic plugs to prevent drying, the sample tube was connected to the piezo actuator (*Figure 1D*) and inserted into the magnet of the scanner (*Figure 2*). MRE examination was initiated within 30 minutes of specimen resection in all cases included in this study.

MRE

As described in detail in the study by Braun *et al.* (41), a

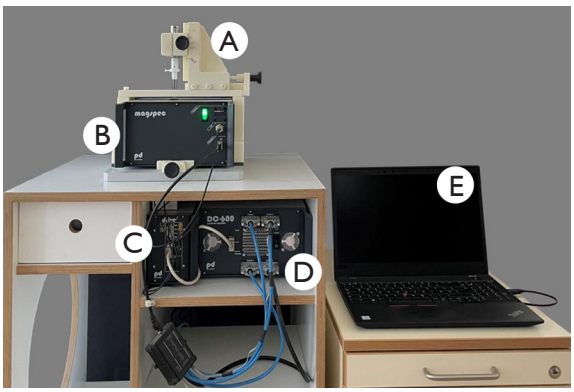

Figure 2 Setup of the Benchtop MRI scanner customized for automated MRE exams. (A) Mounting for the piezo-based driver with inserted sample tube (see also *Figure 1D*). (B) 0.5-T permanent magnet. (C) MRI control unit. (D) External gradient amplifier supplying imaging gradients and piezo driver. (E) Computer for scanner control and image calculation. MRI, magnetic resonance imaging; MRE, magnetic resonance elastography.

tabletop MRI scanner (Pure Devices GmbH, Würzburg, Germany) with a 0.5-T permanent magnet with a 10-mm bore was customized for MRE by a four-channel external gradient amplifier (DC 600, Pure Devices GmbH, Würzburg, Germany) and an integrated MRI system-controlled piezoelectrical driver (Piezosystem Jena GmbH, Jena, Germany). The vibration frequencies used for shear wave induction were empirically determined in a preparatory examination based on the mechanical properties of ileum. The lower frequency limit was chosen so that the observed shear wavelength was approximately equal to the radius of the test tube. The upper frequency limit was determined by the damping property of the tissue so at least one shear wavelength was visible. These limits resulted in frequencies f of 1,000, 1,500, 2,000, 2,500, and 3,000 Hz which were consecutively induced from the walls of the sample tube, generating concentric shear waves emanating towards the center of the tissue. Wave images were acquired using a spin-echo-based MRE sequence (41) with trapezoidal bipolar motion-encoding gradients (MEGs) of 0.2 T/m amplitude, polarized along the cylinder axis (thru-plane) and synchronized to vibration frequency f; 20 ms encoding time was set for all frequencies, resulting in a variable number of MEG cycles from 20 to 60 for frequencies from f=1,000 to 3,000, respectively. Further acquisition parameters were: repetition time (TR): 700 ms, echo time (TE): 30 ms, field of view (FoV): 9.6×9.6 mm^2, matrix size: 64×64, in-plane resolution: 150×150 µm^2, and slice thickness: 3.0 mm. The total acquisition time for all 5 vibration frequencies, each of which sampled with 4 wave dynamics, was approximately 15 min per sample.

According to the study by Tzschätzsch *et al.* (43), shear wave speed (c in m/s) and penetration rate (a in m/s) as markers of stiffness and viscosity were calculated by fitting the analytical solution of shear waves in a z-infinite cylinder (44) from the complex-valued wave images after phase unwrapping and temporal Fourier transformation. Damping ratio $\gamma=G''/2G'$, with G' and G'' denoting the real and imaginary part of the complex shear modulus G^*, was derived from c and a by:

$$G^* = \frac{\rho}{\left(\frac{1}{c} - i\frac{1}{2\pi a}\right)^2} \quad [1]$$

with the density ρ of the tissue samples (1,000 kg/m^3) (5,45). Additionally, frequency-independent viscosity η and dimensionless power-law exponent α were derived from the dispersion of c and a using Eq. [1] and the two-parameter viscoelastic spring-pot model (5):

$$G^* = \mu^{1-\alpha}\eta^{\alpha}(i\omega)^{\alpha} \quad [2]$$

Here, μ and η represent linearly dependent fit variables, which can be converted to an independent parameter of elasticity or viscosity by assuming either a specific viscosity or shear modulus (5). Further information and an introductory overview of the current state of development of elastography including preclinical as well as clinical applications can be found in the study by Sack (45).

Statistical analysis

Values were reported as median ± mean absolute deviation (MAD). The MAD indicates how far the samples deviate from their median on average and is calculated as follows:

$$MAD = \frac{1}{n}\sum_{i=1}^{n}|x_i - \bar{x}| \quad [3]$$

with n elements and the median $\bar{x}$ of the sample. A two-sided Wilcoxon rank sum test (Matlab Statistics and Machine Learning toolbox R2020b, The MathWorks, Inc., Natick, Massachusetts, USA) was applied for the comparison of continuous distributions with equal medians. For calculation of the diagnostic accuracy of the respective viscoelastic parameters, area under the receiver operating

Table 1 Demographic and clinical characteristics of patients

Characteristics	Number
Patients	12
CD	7
Control group	5
Age	
Median age (years)	48
Age range (years)	34–68
Sex, n (%)	
Female	6 (50.0)
Male	6 (50.0)
Time between initial diagnosis of CD and surgery	
Median (years)	18
Range (years)	16–37
Medical therapy for CD at time of surgery, n (%)	
Prednisone	2 (28.6)
Mesalazin	1 (14.3)
Azathioprine & antibodies (adalimumab, infliximab)	2 (28.6)
None	2 (28.6)

CD, Crohn's disease.

characteristic curve (AUC) analysis with 95% confidence interval (CI) was performed (IBM SPSS Statistics for Windows, Version 25.0, IBM Corp., Armonk, New York, USA). For significance testing, a P value <0.05 was considered to indicate a statistically significant difference.

Results

Demographic and clinical characteristics of the patients included are summarized in *Table 1*. For healthy ileum and ileum affected by CD, shear wave speeds c and shear wave penetration rates a were calculated for all vibration frequencies from the respective complex wave images (*Figure 3*) by fitting to the averaged radial profile of the complex wave field maps. Visual inspection alone already revealed consistent differences with a higher penetration rate for ileum samples affected by CD while no apparent oscillations were visible, indicating critical damping (17). *Table 2* summarizes all frequency-dependent values of c, a, and damping ratio γ. *Figure 4* shows group values of c, a, and γ for all vibration frequencies for ileum affected by CD and the control group of healthy ileum. Specimens affected by CD were found to have a significantly lower viscosity-related penetration rate a (*Figure 4A*) than healthy ileum ($P<0.05$) for all vibration frequencies, reflecting a higher viscous attenuation. Consistently, damping ratio γ was higher in CD than healthy specimens, both averaged over all frequencies (healthy: 0.58±0.12, CD: 1.04±0.55, P=0.03) and with significance at 1,000 and 1,500 Hz (*Figure 4B*). No significant difference was observed for stiffness-related c (*Figure 4C*) between healthy ileum and ileum affected by CD at any frequency.

Figure 5 presents the analysis of the frequency dispersion of c and a for one sample each of healthy (*Figure 5A*) and CD-affected tissue (*Figure 5B*), obtained by fitting the rheological spring-pot model to the experimental data. This fractional power-law model (5) is based on two independent parameters when assuming a specific shear modulus (μ=1 kPa): (I) the dimensionless power-law exponent α that ranges between 0 (the limit of elastic-solid behavior) and 1 (the limit of viscous-fluid behavior) and (II) the viscosity-related parameter η with the unit of Pa·s. Values of α and η are also summarized in *Table 2*. The power-law exponent α in CD-affected ileum (α=0.73±0.06) was significantly higher compared to healthy ileum (α=0.55±0.05, P=0.02, *Figure 6A*). Additionally, with values larger than 0.5, α indicated predominantly viscous properties of both healthy and CD-affected ileum. Consistent with our frequency-resolved analysis of penetration rates a and damping ratio γ, the spring-pot model showed η to be significantly reduced in CD-affected tissue compared to healthy control tissue (2.62±1.37 *vs.* 10.60±12.60 Pa·s, P=0.02) (*Figure 6B*).

Diagnostic accuracy for the prediction of CD was calculated based on a with an AUC of 0.94 (95% CI: 0.81–1.00) at 1,000 Hz, 1.00 (95% CI: 1.00–1.00) at 1,500 Hz, 0.91 (95% CI: 0.74–1.00) at 2,000 Hz and 0.86 (95% CI: 0.62–1.00) at 2,500 Hz and 0.86 (95% CI: 0.64–1.00) at 3,000 Hz ($P<0.05$). Based on η, diagnostic accuracy for the prediction of CD was AUC =1.00 (95% CI: 1.00–1.00, $P<0.01$).

Discussion

To the best of our knowledge, this is the first study investigating resected intestinal sections from CD patients using multifrequency MRE and analyzing elastic and viscous tissue properties. The setup we used in this study was less biased than other inversion-based MRE techniques (46) due to the cylinder geometry of the samples and the noise-insensitive, analytical solution for elasticity reconstruction.

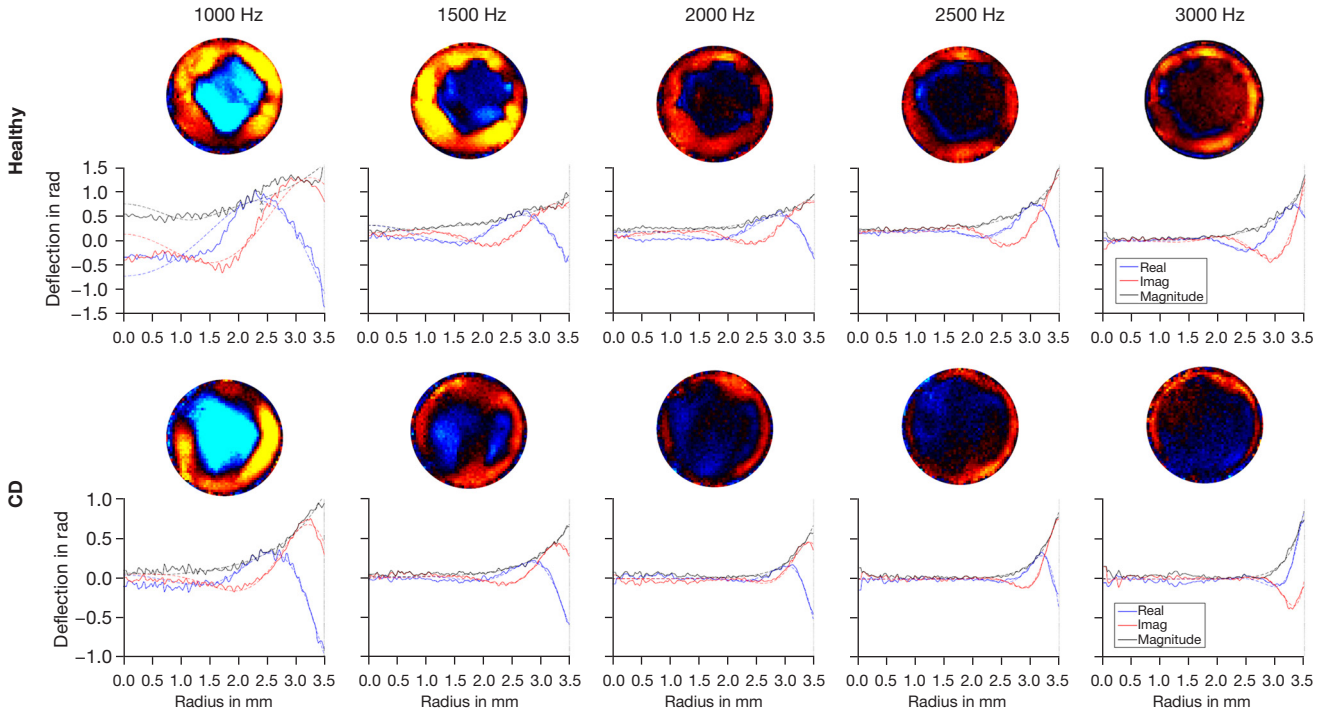

Figure 3 Experimental wave images and fit of wave numbers. For healthy tissue (top two rows) and tissue affected by CD (bottom two rows), the real part of the complex-valued wave images after unwrapping and temporal Fourier transformation are depicted for all vibration frequencies, respectively. Fits of complex wave profiles based on Bessel functions are shown below the wave images. From the fitted complex wave number shear wave speed c and penetration rate a are calculated. Already by visual inspection, consistent differences of a decreased penetration rate (higher damping) for CD affected ileum can be identified. CD, Crohn's disease.

Table 2 Summary of calculated viscoelastic parameters for each specimen

Pat-ID	*c* in m/s					*a* in m/s					Damping ratio γ					Spring-pot model	
	1,000	1,500	2,000	2,500	3,000	1,000	1,500	2,000	2,500	3,000	1,000	1,500	2,000	2,500	3,000	η in Pa·s	α
Healthy ileum																	
1	3.52	3.61	4.36	4.55	4.92	1.34	1.50	1.55	1.41	1.53	0.51	0.45	0.56	0.70	0.69	10.60	0.55
2	4.32	4.89	5.45	5.43	5.61	1.68	1.67	2.04	2.21	1.59	0.49	0.60	0.52	0.46	0.82	29.22	0.53
3	4.28	4.72	4.53	4.49	4.63	1.57	1.53	1.18	1.06	1.05	0.53	0.65	0.98	1.24	1.38	8.56	0.59
4	5.17	5.37	5.15	5.14	5.25	1.71	1.79	2.03	2.11	1.94	0.63	0.62	0.48	0.46	0.53	48.93	0.49
5	3.52	3.88	4.73	4.97	5.81	1.43	1.44	1.34	1.42	1.37	0.46	0.53	0.82	0.81	1.24	6.06	0.65
Ileum affected by CD																	
6	1.50	1.41	2.21	2.06	2.71	0.47	0.42	0.74	0.58	0.61	0.51	0.45	0.56	0.70	0.69	0.35	0.73
7	2.54	2.80	3.18	3.19	3.90	0.73	0.80	0.72	0.79	0.76	0.49	0.60	0.52	0.46	0.82	1.10	0.74
8	3.90	5.41	6.91	6.49	7.06	1.54	1.41	1.65	1.42	1.45	0.53	0.65	0.98	1.24	1.38	5.43	0.77
9	3.99	4.44	5.31	5.41	5.31	1.17	0.78	0.91	1.01	1.03	0.63	0.62	0.48	0.46	0.53	2.62	0.79
10	3.84	4.30	4.13	5.31	5.00	1.13	1.10	0.98	1.21	1.40	0.46	0.53	0.82	0.81	1.24	4.36	0.68
11	2.60	3.17	3.31	3.66	3.56	0.82	0.92	0.95	1.09	0.94	0.51	0.45	0.56	0.70	0.69	2.31	0.63
12	2.74	2.68	3.95	3.38	3.61	0.85	1.04	1.14	1.22	1.11	0.49	0.60	0.52	0.46	0.82	3.58	0.58

CD, Crohn's disease.

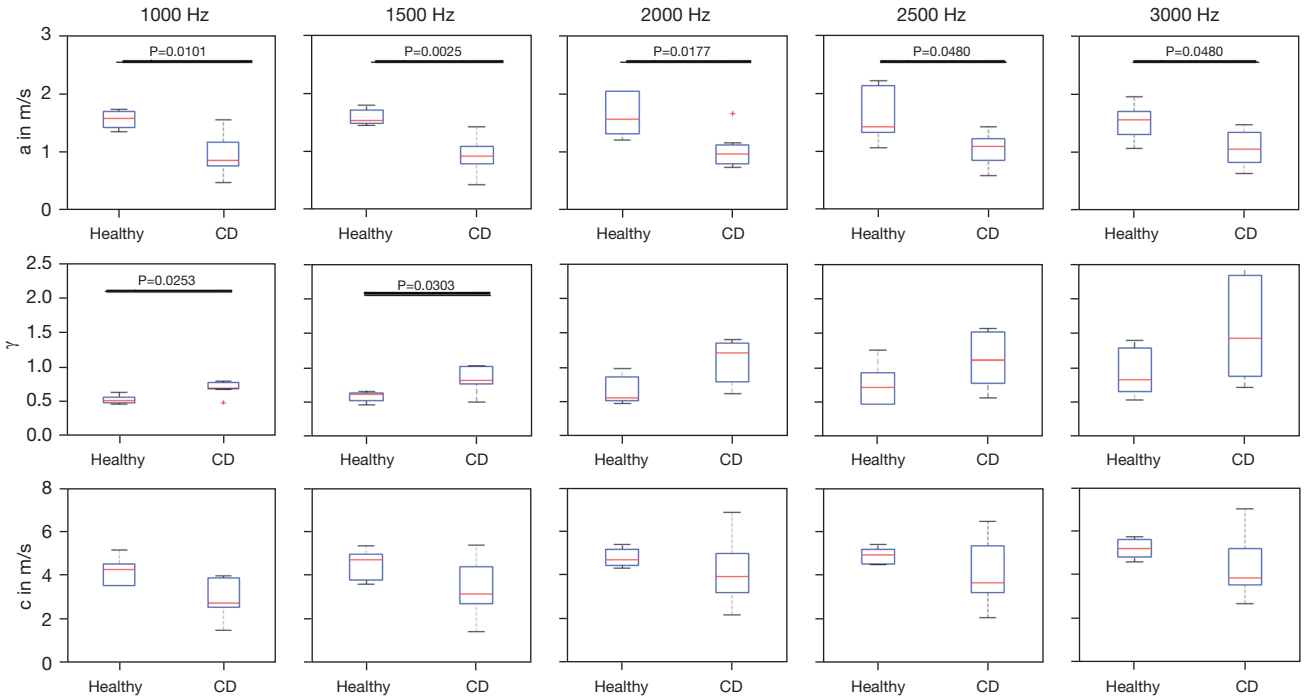

Figure 4 Boxplots of frequency-dependent parameters for the groups of healthy and CD-affected ileum for all vibration frequencies. (A) Shear wave penetration rate *a*. (B) Damping ratio *γ*. (C) Shear wave speed *c*. Significant differences between the groups were found for *a* and damping ratio *γ* as indicated by bars with associated P values. CD, Crohn's disease.

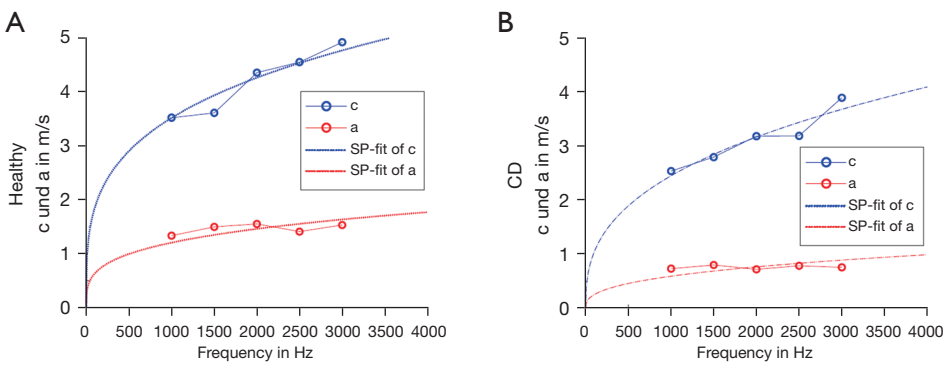

Figure 5 Rheological modeling of the frequency dispersion of shear wave speed *c* and penetration rate *a*. (A) Representative sample of healthy tissue. (B) Representative sample of CD-affected tissue. The solid curves of the fits to *c* and *a* are parameterized by the two independent parameters viscosity *η* and structure parameter *α* of the spring-pot model (see Methods section). SP, spring-pot; CD, Crohn's disease.

The consistency of our method was confirmed in a well-characterized tissue-mimicking phantom providing values in agreement with shear oscillatory rheometry (47). Due to this consistency, tabletop MRE was used in previous studies (41,48-50) as a reference method and was employed here without further calibration. Shear wave speed *c*, shear wave penetration rate *a*, and damping ratio *γ* were determined as surrogate markers of stiffness, viscosity, and dissipation, respectively. Tissue areas affected by CD showed a lower penetration rate and higher damping ratio than areas without CD. Consistent with the observed higher spring-pot-based viscosity and power-law exponent, these findings suggest that viscous properties of ileum tissue are significantly altered in the presence of CD. In patients,

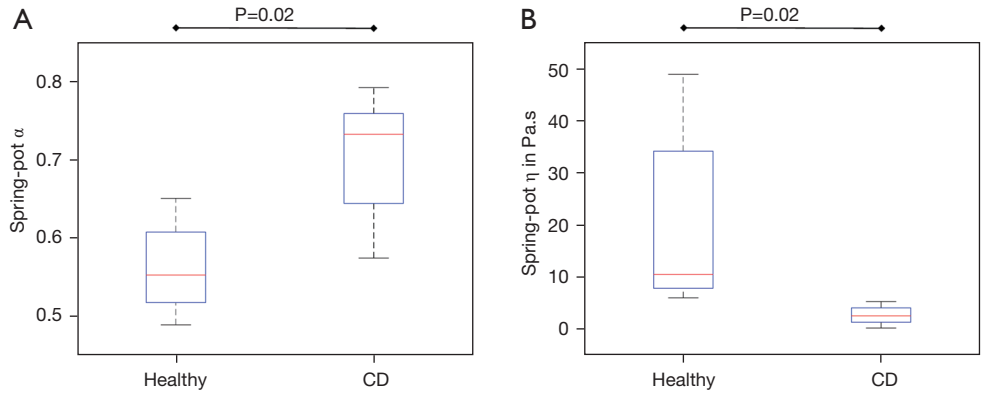

Figure 6 Boxplots of the two frequency-independent spring-pot model parameters for the groups of healthy and CD affected ileum. (A) Dimensionless power-law exponent α. (B) Viscosity-related parameter η. Both show significant differences indicated by bars with corresponding P values. CD, Crohn's disease.

MRE measures values that can be converted to the higher frequency range used in this study by using viscoelastic models (45). MRE in chronic IBDs was performed in a frequency range between 40 and 70 Hz and based on tomoelastography reconstruction (37).

Compared to MRE findings reported in the literature for other soft tissues, we observed an unusually high damping ratio of γ>0.5 in healthy samples and even exceeding 1 in CD specimens, suggesting critical damping of the induced oscillations. Lower values on the order of γ=0.22 were reported for brain tissue (51) in the lower frequency range of *in vivo* MRE (60 Hz) while *c* and *a* values reported for liver tissue in a similar frequency range as used in our study were around 0.35 (52). This marked dissipative behavior of intestinal tissue seems to reflect the functional property of mechanical flexibility and mucus production of intestinal walls.

The lower penetration rate we observed in inflamed intestinal tissue is consistent with published data. Marticorena *et al.* (35) showed a significantly increased loss angle (which his related to γ) in acute appendicitis, consistent with Reiter *et al.* (37), who showed an increased loss angle in patients with IBD. A direct comparison of quantitative values obtained with *in vivo* MRE and tabletop MRE is hampered by the different frequency ranges. Especially, soft tissues with predominantly viscous properties, such as the ileum specimens investigated in our study, display marked dispersion of shear wave speed and wave penetration, resulting in higher values at higher frequencies.

Published data indicate that a change in viscosity of soft tissues due to inflammation seems to correspond to an active early stage of inflammatory responses whereas changes in stiffness occur during a chronic fibrotic stage (36,38,40). Both in CD-related fibrogenesis and in liver fibrosis, active inflammatory responses precede fibrosis (53,54). However, in most intestinal areas affected by CD, the nature of affection is mixed (3). Thus, in predominantly chronic disease (i.e., fibrosis), there is usually some level of active inflammation and vice versa. Consistent with the significant change in viscosity we observed here, all ileum samples affected by CD used in our study showed primarily active inflammatory aspects of CD manifestation based on macroscopic evaluation by the study surgeon. On the other hand, the long median interval between initial diagnosis of CD and surgery of 18 years in our study patients makes chronic changes such as fibrosis with higher stiffness very likely. In Reiter *et al.* (37), this aspect appears to be reflected by an increase in stiffness that accompanies the changes of viscous attenuation in the investigated tissue affected by CD. In contrast, in the present study, differences in *c* did not reach significance, which is consistent with the results of some USE studies. While Baumgart *et al.* (6) also observed higher stiffness in regions affected by CD, Chen *et al.* (11), Serra *et al.* (10), and Lu *et al.* (13) did not observe a correlation of stiffness with fibrosis scores. Instead, Lu *et al.* (13) found increased stiffness of intestinal walls to correlate with smooth muscle hypertrophy. As smooth muscle hypertrophy plays a major role in the development of fibrostenotic CD (55), the lack of muscle activity in our *ex vivo* specimens could explain that tissue stiffness was not significantly altered. Overall, these results underline the need to systematically investigate different confounding factors that influence viscoelastic parameters in intestinal tissues altered by CD.

Beyond stiffness, our study provides evidence that viscosity is a potentially sensitive imaging marker in CD. The accuracy for diagnosing the involvement of CD in terminal ileum was good (AUC ≥0.86) to high (AUC =1.00) for frequency-averaged a and spring-pot-based η, respectively. This analysis is consistent with AUC =0.84 for the diagnosis of IBD by *in vivo* MRE based on the loss angle of the complex modulus (37).

Although we obtained encouraging results, the present study has limitations. First, we did not perform histological characterization and quantification, which limits our interpretation of parameter changes with respect to inflammation and fibrosis. Next, our group sizes were small. Investigation of larger groups combined with histopathological analysis would improve the statistical power of the results and better allow to disentangle the respective effects of active inflammation and fibrosis on stiffness and viscosity. However, intraoperative macroscopic evaluation by the surgeon is a standard procedure to define the extent of CD affection of the ileum providing the reference standard in our study.

Nevertheless, this study shows MRE to be a sensitive tool for analyzing the viscoelastic properties of small bowel specimens immediately after surgical removal. Strikingly, bowel tissue exhibits markedly viscous and dissipative mechanical properties, resulting in critically damped shear waves in a frequency range between 1 and 3 kHz. Even with the small number of examinations we performed, wave penetration, damping ratio, and spring-pot-based viscosity consistently showed ileum affected by CD to be markedly more viscous and dissipative than healthy ileum. This demonstrates the capability of MRE to sensitively quantify significant differences in viscoelastic parameters between healthy ileum and ileum affected by CD.

In this way, our work demonstrates the potential of MRE as an imaging technique to complement conventional magnetic resonance enterography in the characterization of CD lesions and provide additional information for better therapeutic decision-making. On this basis, future studies are warranted with comprehensive *in vivo* and subsequent *ex vivo* MRE mapping and histopathological correlation including characterization and exact quantification of inflammation and fibrosis.

Conclusions

MRE is feasible and able to determine viscoelastic properties of small bowel and, furthermore, to quantify differences in viscoelastic properties between healthy terminal ileum and terminal ileum affected by CD.

Acknowledgments

Funding: This study was funded by the Deutsche Forschungsgemeinschaft (DFG, German Research Foundation): Project CRC 1340 Matrix in Vision (to Patrick Asbach, Ingolf Sack, and Jürgen Braun).

Footnote

Conflicts of Interest: All authors have completed the ICMJE uniform disclosure form (available at https://qims.amegroups.com/article/view/10.21037/qims-22-1071/coif). PA, IS, and JB received funding by the Deutsche Forschungsgemeinschaft (DFG, German Research Foundation): Project CRC 1340 Matrix in Vision. The other authors have no conflicts of interest to declare.

Ethical Statement: The authors are accountable for all aspects of the work in ensuring that questions related to the accuracy or integrity of any part of the work are appropriately investigated and resolved. The study was conducted in accordance with the Declaration of Helsinki (as revised in 2013). The study was approved by the ethics committee of the Charité – Universitätsmedizin Berlin (No. EA4/007/19), and written informed consent was obtained from each patient.

References

1. Feuerstein JD, Cheifetz AS. Crohn Disease: Epidemiology, Diagnosis, and Management. Mayo Clin Proc 2017;92:1088-103.
2. The global, regional, and national burden of inflammatory bowel disease in 195 countries and territories, 1990-2017: a systematic analysis for the Global Burden of Disease

Study 2017. Lancet Gastroenterol Hepatol 2020;5:17-30.
3. Rieder F, Zimmermann EM, Remzi FH, Sandborn WJ. Crohn's disease complicated by strictures: a systematic review. Gut 2013;62:1072-84.
4. Maaser C, Sturm A, Vavricka SR, Kucharzik T, Fiorino G, Annese V, et al. ECCO-ESGAR Guideline for Diagnostic Assessment in IBD Part 1: Initial diagnosis, monitoring of known IBD, detection of complications. J Crohns Colitis 2019;13:144-64.
5. Hirsch S, Braun J, Sack I. Magnetic resonance elastography: physical background and medical applications. Weinheim: Wiley-VCH Verlag GmbH & Co. KGaA; 2016:426.
6. Baumgart DC, Müller HP, Grittner U, Metzke D, Fischer A, Guckelberger O, Pascher A, Sack I, Vieth M, Rudolph B. US-based Real-time Elastography for the Detection of Fibrotic Gut Tissue in Patients with Stricturing Crohn Disease. Radiology 2015;275:889-99.
7. Ding SS, Fang Y, Wan J, Zhao CK, Xiang LH, Liu H, Pu H, Xu G, Zhang K, Xu XR, Sun XM, Liu C, Wu R. Usefulness of Strain Elastography, ARFI Imaging, and Point Shear Wave Elastography for the Assessment of Crohn Disease Strictures. J Ultrasound Med 2019;38:2861-70.
8. Lo Re G, Picone D, Vernuccio F, Scopelliti L, Di Piazza A, Tudisca C, Serraino S, Privitera G, Midiri F, Salerno S, Midiri M, Bartolotta TV, Lagalla R. Comparison of US Strain Elastography and Entero-MRI to Typify the Mesenteric and Bowel Wall Changes during Crohn's Disease: A Pilot Study. Biomed Res Int 2017;2017:4257987.
9. Quaia E, Gennari AG, van Beek EJR. Differentiation of Inflammatory from Fibrotic Ileal Strictures among Patients with Crohn's Disease through Analysis of Time-Intensity Curves Obtained after Microbubble Contrast Agent Injection. Ultrasound Med Biol 2017;43:1171-8.
10. Serra C, Rizzello F, Pratico' C, Felicani C, Fiorini E, Brugnera R, Mazzotta E, Giunchi F, Fiorentino M, D'Errico A, Morselli-Labate AM, Mastroroberto M, Campieri M, Poggioli G, Gionchetti P. Real-time elastography for the detection of fibrotic and inflammatory tissue in patients with stricturing Crohn's disease. J Ultrasound 2017;20:273-84.
11. Chen YJ, Mao R, Li XH, Cao QH, Chen ZH, Liu BX, Chen SL, Chen BL, He Y, Zeng ZR, Ben-Horin S, Rimola J, Rieder F, Xie XY, Chen MH. Real-Time Shear Wave Ultrasound Elastography Differentiates Fibrotic from Inflammatory Strictures in Patients with Crohn's Disease. Inflamm Bowel Dis 2018;24:2183-90.
12. Goertz RS, Lueke C, Wildner D, Vitali F, Neurath MF, Strobel D. Acoustic radiation force impulse (ARFI) elastography of the bowel wall as a possible marker of inflammatory activity in patients with Crohn's disease. Clin Radiol 2018;73:678.e1-5.
13. Lu C, Gui X, Chen W, Fung T, Novak K, Wilson SR. Ultrasound Shear Wave Elastography and Contrast Enhancement: Effective Biomarkers in Crohn's Disease Strictures. Inflamm Bowel Dis 2017;23:421-30.
14. Thimm MA, Cuffari C, Garcia A, Sidhu S, Hwang M. Contrast-Enhanced Ultrasound and Shear Wave Elastography Evaluation of Crohn's Disease Activity in Three Adolescent Patients. Pediatr Gastroenterol Hepatol Nutr 2019;22:282-90.
15. Abe H, Midorikawa Y, Higaki T, Yamazaki S, Aramaki O, Nakayama H, Moriguchi M, Kanda T, Moriyama M, Okada M, Nishimaki H, Sugitani M, Tsuji S, Takayama T. Magnetic resonance elastography-based prediction of hepatocellular carcinoma recurrence after curative resection. Surgery 2021;170:167-72.
16. Guo J, Büning C, Schott E, Kröncke T, Braun J, Sack I, Althoff CE. In vivo abdominal magnetic resonance elastography for the assessment of portal hypertension before and after transjugular intrahepatic portosystemic shunt implantation. Invest Radiol 2015;50:347-51.
17. Manduca A, Bayly PJ, Ehman RL, Kolipaka A, Royston TJ, Sack I, Sinkus R, Van Beers BE. MR elastography: Principles, guidelines, and terminology. Magn Reson Med 2021;85:2377-90.
18. Reiter R, Shahryari M, Tzschätzsch H, Haas M, Bayerl C, Siegmund B, Hamm B, Asbach P, Braun J, Sack I. Influence of fibrosis progression on the viscous properties of in vivo liver tissue elucidated by shear wave dispersion in multifrequency MR elastography. J Mech Behav Biomed Mater 2021;121:104645.
19. Shahryari M, Tzschätzsch H, Guo J, Marticorena Garcia SR, Böning G, Fehrenbach U, Stencel L, Asbach P, Hamm B, Käs JA, Braun J, Denecke T, Sack I. Tomoelastography Distinguishes Noninvasively between Benign and Malignant Liver Lesions. Cancer Res 2019;79:5704-10.
20. Singh R, Wilson MP, Katlariwala P, Murad MH, McInnes MDF, Low G. Accuracy of liver and spleen stiffness on magnetic resonance elastography for detecting portal hypertension: a systematic review and meta-analysis. Eur J Gastroenterol Hepatol 2021;32:237-45.
21. Tapper EB, Loomba R. Noninvasive imaging biomarker assessment of liver fibrosis by elastography in NAFLD.

Nat Rev Gastroenterol Hepatol 2018;15:274-82.
22. Zhou JH, Cai JJ, She ZG, Li HL. Noninvasive evaluation of nonalcoholic fatty liver disease: Current evidence and practice. World J Gastroenterol 2019;25:1307-26.
23. Jhang ZE, Wu KL, Chen CB, Chen YL, Lin PY, Chou CT. Diagnostic value of spleen stiffness by magnetic resonance elastography for prediction of esophageal varices in cirrhotic patients. Abdom Radiol (NY) 2021;46:526-33.
24. Kennedy P, Stocker D, Carbonell G, Said D, Bane O, Hectors S, Abboud G, Cuevas J, Bolster BD Jr, Friedman SL, Lewis S, Schiano T, Bhattacharya D, Fischman A, Thung S, Taouli B. MR elastography outperforms shear wave elastography for the diagnosis of clinically significant portal hypertension. Eur Radiol 2022;32:8339-49.
25. Yoon H, Shin HJ, Kim MJ, Han SJ, Koh H, Kim S, Lee MJ. Predicting gastroesophageal varices through spleen magnetic resonance elastography in pediatric liver fibrosis. World J Gastroenterol 2019;25:367-77.
26. Kirpalani A, Hashim E, Leung G, Kim JK, Krizova A, Jothy S, Deeb M, Jiang NN, Glick L, Mnatzakanian G, Yuen DA. Magnetic Resonance Elastography to Assess Fibrosis in Kidney Allografts. Clin J Am Soc Nephrol 2017;12:1671-9.
27. Marticorena Garcia SR, Fischer T, Dürr M, Gültekin E, Braun J, Sack I, Guo J. Multifrequency Magnetic Resonance Elastography for the Assessment of Renal Allograft Function. Invest Radiol 2016;51:591-5.
28. Marticorena Garcia SR, Grossmann M, Lang ST, Tzschätzsch H, Dittmann F, Hamm B, Braun J, Guo J, Sack I. Tomoelastography of the native kidney: Regional variation and physiological effects on in vivo renal stiffness. Magn Reson Med 2018;79:2126-34.
29. Shatil AS, Kirpalani A, Younus E, Tyrrell PN, Krizova A, Yuen DA. Magnetic Resonance Elastography-derived Stiffness Predicts Renal Function Loss and Is Associated With Microvascular Inflammation in Kidney Transplant Recipients. Transplant Direct 2022;8:e1334.
30. Dittmann F, Tzschätzsch H, Hirsch S, Barnhill E, Braun J, Sack I, Guo J. Tomoelastography of the abdomen: Tissue mechanical properties of the liver, spleen, kidney, and pancreas from single MR elastography scans at different hydration states. Magn Reson Med 2017;78:976-83.
31. Gültekin E, Wetz C, Braun J, Geisel D, Furth C, Hamm B, Sack I, Marticorena Garcia SR. Added Value of Tomoelastography for Characterization of Pancreatic Neuroendocrine Tumor Aggressiveness Based on Stiffness. Cancers (Basel) 2021;13:5185.
32. Itoh Y, Takehara Y, Kawase T, Terashima K, Ohkawa Y, Hirose Y, Koda A, Hyodo N, Ushio T, Hirai Y, Yoshizawa N, Yamashita S, Nasu H, Ohishi N, Sakahara H. Feasibility of magnetic resonance elastography for the pancreas at 3T. J Magn Reson Imaging 2016;43:384-90.
33. Liu Y, Wang M, Ji R, Cang L, Gao F, Shi Y. Differentiation of pancreatic ductal adenocarcinoma from inflammatory mass: added value of magnetic resonance elastography. Clin Radiol 2018;73:865-72.
34. Xu Y, Cai X, Shi Y, Yin M, Lan G, Zhang X, Ji R, Chang Liu. Normative Pancreatic Stiffness Levels and Related Influences Established by Magnetic Resonance Elastography in Volunteers. J Magn Reson Imaging 2020;52:448-58.
35. Marticorena Garcia SR, Hamm B, Sack I. Tomoelastography for non-invasive detection and treatment monitoring in acute appendicitis. BMJ Case Rep 2019. BMJ Case Rep 2019;12:e230791.
36. Avila F, Caron B, Hossu G, Ambarki K, Kannengiesser S, Odille F, Felblinger J, Danese S, Choukour M, Laurent V, Peyrin-Biroulet L. Magnetic Resonance Elastography for Assessing Fibrosis in Patients with Crohn's Disease: A Pilot Study. Dig Dis Sci 2022;67:4518-24.
37. Reiter R, Loch FN, Kamphues C, Bayerl C, Marticorena Garcia SR, Siegmund B, Kühl AA, Hamm B, Braun J, Sack I, Asbach P. Feasibility of Intestinal MR Elastography in Inflammatory Bowel Disease. J Magn Reson Imaging 2022;55:815-22.
38. Garteiser P, Doblas S, Van Beers BE. Magnetic resonance elastography of liver and spleen: Methods and applications. NMR Biomed 2018;31:e3891.
39. Shi Y, Qi YF, Lan GY, Wu Q, Ma B, Zhang XY, Ji RY, Ma YJ, Hong Y. Three-dimensional MR Elastography Depicts Liver Inflammation, Fibrosis, and Portal Hypertension in Chronic Hepatitis B or C. Radiology 2021;301:154-62.
40. Yin M, Glaser KJ, Manduca A, Mounajjed T, Malhi H, Simonetto DA, Wang R, Yang L, Mao SA, Glorioso JM, Elgilani FM, Ward CJ, Harris PC, Nyberg SL, Shah VH, Ehman RL. Distinguishing between Hepatic Inflammation and Fibrosis with MR Elastography. Radiology 2017;284:694-705.
41. Braun J, Tzschätzsch H, Körting C, Ariza de Schellenberger A, Jenderka M, Drießle T, Ledwig M, Sack I. A compact 0.5 T MR elastography device and its application for studying viscoelasticity changes in biological tissues during progressive formalin fixation. Magn Reson Med 2018;79:470-8.
42. Everwien H, Ariza de Schellenberger A, Haep N, Tzschätzsch H, Pratschke J, Sauer IM, Braun J,

Hillebrandt KH, Sack I. Magnetic resonance elastography quantification of the solid-to-fluid transition of liver tissue due to decellularization. J Mech Behav Biomed Mater 2020;104:103640.
43. Tzschätzsch H, Guo J, Dittmann F, Hirsch S, Barnhill E, Jöhrens K, Braun J, Sack I. Tomoelastography by multifrequency wave number recovery from time-harmonic propagating shear waves. Med Image Anal 2016;30:1-10.
44. Yasar TK, Royston TJ, Magin RL. Wideband MR elastography for viscoelasticity model identification. Magn Reson Med 2013;70:479-89.
45. Sack I. Magnetic resonance elastography from fundamental soft-tissue mechanics to diagnostic imaging. Nat Rev Phys 2022;5:25-42.
46. Mura J, Schrank F, Sack I. An analytical solution to the dispersion-by-inversion problem in magnetic resonance elastography. Magn Reson Med 2020;84:61-71.
47. Morr AS, Herthum H, Schrank F, Görner S, Anders MS, Lerchbaumer M, Müller HP, Fischer T, Jenderka KV, Hansen HHG, Janmey PA, Braun J, Sack I, Tzschätzsch H. Liquid-Liver Phantom: Mimicking the Viscoelastic Dispersion of Human Liver for Ultrasound- and MRI-Based Elastography. Invest Radiol 2022;57:502-9.
48. Bertalan G, Guo J, Tzschätzsch H, Klein C, Barnhill E, Sack I, Braun J. Fast tomoelastography of the mouse brain by multifrequency single-shot MR elastography. Magn Reson Med 2019;81:2676-87.
49. Jordan JEL, Bertalan G, Meyer T, Tzschätzsch H, Gauert A, Bramè L, Herthum H, Safraou Y, Schröder L, Braun J, Hagemann AIH, Sack I. Microscopic multifrequency MR elastography for mapping viscoelasticity in zebrafish. Magn Reson Med 2022;87:1435-45.
50. Zampini MA, Guidetti M, Royston TJ, Klatt D. Measuring viscoelastic parameters in Magnetic Resonance Elastography: a comparison at high and low magnetic field intensity. J Mech Behav Biomed Mater 2021;120:104587.
51. McIlvain G, Schwarb H, Cohen NJ, Telzer EH, Johnson CL. Mechanical properties of the in vivo adolescent human brain. Dev Cogn Neurosci 2018;34:27-33.
52. Garczyńska K, Tzschätzsch H, Kühl AA, Morr AS, Lilaj L, Häckel A, Schellenberger E, Berndt N, Holzhütter HG, Braun J, Sack I, Guo J. Changes in Liver Mechanical Properties and Water Diffusivity During Normal Pregnancy Are Driven by Cellular Hypertrophy. Front Physiol 2020;11:605205.
53. Burke JP, Mulsow JJ, O'Keane C, Docherty NG, Watson RW, O'Connell PR. Fibrogenesis in Crohn's disease. Am J Gastroenterol 2007;102:439-48.
54. Friedman SL. Mechanisms of hepatic fibrogenesis. Gastroenterology 2008;134:1655-69.
55. Li J, Mao R, Kurada S, Wang J, Lin S, Chandra J, Rieder F. Pathogenesis of fibrostenosing Crohn's disease. Transl Res 2019;209:39-54.

Cite this article as: Loch FN, Kamphues C, Beyer K, Schineis C, Asbach P, Reiter R, Sack I, Braun J. *Ex vivo* magnetic resonance elastography of the small bowel in Crohn's disease. Quant Imaging Med Surg 2023;13(5):2895-2906. doi: 10.21037/qims-22-1071

